water

MDPI

Article

Preparation of a Novel Activated Carbon from Cassava Sludge for the High-Efficiency Adsorption of Hexavalent Chromium in Potable Water: Adsorption Performance and Mechanism Insight

Ling Li [1,†], Yan Li [1,†], Yiqi Liu [1], Lei Ding [1,2,*], Xiaopeng Jin [1], Hongwei Lian [2,3] and Jun Zheng [2,3,*]

[1] School of Civil Engineering and Architecture, Anhui University of Technology, Maanshan 243002, China; leeling970202@163.com (L.L.); yanli20@ahut.edu.cn (Y.L.); lyq3618199@126.com (Y.L.); 1835512810m0@sina.cn (X.J.)
[2] Engineering Research Center of Biofilm Water Purification and Utilization Technology, Ministry of Education, Anhui University of Technology, Maanshan 243002, China; lianhongwei@huaqitech.com.cn
[3] Anhui Huaqi Environmental Protection Technology Co., Ltd., Maanshan 243032, China
* Correspondence: dllyan@ahut.edu.cn (L.D.); zhengjun@huaqitech.com.cn (J.Z.); Tel.: +86-189-4963-3382 (L.D.); +86-189-0555-0033 (J.Z.)
† These two authors contributed equally to this work.

Abstract: Particularly, because of the leakage risk of metal elements from sludge carbon, little attention has been focused on using sludge activated carbon as an adsorbent for the removal of Cr (VI) from contaminated water sources. Herein, a novel sludge carbon derived from dewatered cassava sludge was synthesized by pyrolysis using $ZnCl_2$ as an activator at the optimal conditions. The prepared sludge activated carbon possessed a large BET surface (509.03 m^2/g), demonstrating an efficient removal for Cr (VI). Although the time to reach equilibrium was extended by increasing the initial Cr (VI) concentration, the adsorption process was completed within 3 h. The kinetics of adsorption agreed with the Elovich model. The whole adsorption rate was controlled by both film and intra-particle diffusion. The Cr (VI) removal efficiency increased with elevating temperature, and the adsorption equilibrium process followed the Freundlich isotherm model. The adsorption occurred spontaneously with endothermic nature. The removal mechanism of Cr (VI) on the prepared sludge activated carbon depended highly on solution pH, involving pore filling, electrostatic attraction, reduction, and ion exchange. The trace leakage of metal elements after use was confirmed. Therefore, the prepared sludge activated carbon was considered to be a highly potential adsorbent for Cr (VI) removal from contaminated raw water.

Keywords: sludge activated carbon; Cr (VI); adsorption; drinking water treatment; mechanism

check for updates

Citation: Li, L.; Li, Y.; Liu, Y.; Ding, L.; Jin, X.; Lian, H.; Zheng, J. Preparation of a Novel Activated Carbon from Cassava Sludge for the High-Efficiency Adsorption of Hexavalent Chromium in Potable Water: Adsorption Performance and Mechanism Insight. *Water* **2021**, *13*, 3602. https://doi.org/10.3390/13243602

Academic Editor: Laura Bulgariu

Received: 20 November 2021
Accepted: 13 December 2021
Published: 15 December 2021

Publisher's Note: MDPI stays neutral with regard to jurisdictional claims in published maps and institutional affiliations.

Copyright: © 2021 by the authors. Licensee MDPI, Basel, Switzerland. This article is an open access article distributed under the terms and conditions of the Creative Commons Attribution (CC BY) license (https://creativecommons.org/licenses/by/4.0/).

1. Introduction

Hexavalent chromium (Cr (VI)) has been widely applied in petroleum, oil refining, electroplating, tanning, metallurgy, fertilizer, and other industrial processes [1,2]. Over the past two decades in many developing countries, raw water sources have been frequently contaminated by wastewater and solid waste containing Cr (VI) due to abnormal discharge [3]. The total Cr (VI) in potable water has been limited within the range of 0.05 mg/L by WHO due to its carcinogenicity, teratogenicity, and mutagenicity [4]. For raw water contaminated by Cr (VI) due to sudden pollution accidents, traditional drinking water treatment processes, comprising coagulation, sedimentation, filtration, and disinfection, are poorly effective for Cr (VI) removal. For example, local potable water treatment plants were closed for nearly ten days due to water pollution caused by Cr (VI) in Qujing city, China [3]. Hence, it is essential to search for a high-efficiency treatment technology to remove Cr (VI) from contaminated raw water sources.

For eliminating Cr (VI) from industrial wastewater, many researchers have reported different technologies, such as bioremediation [5], reduction-coagulation (chemical or

electrochemical) [6,7], membrane separation [8], and ion exchange [9]. However, few studies were concerned with the removal of Cr (VI) from raw water sources contaminated by sudden water pollution accidents. In drinking water treatment plants, divalent iron salt, such as ferrous sulfate ($FeSO_4$) or ferrous chloride ($FeCl_2$), is often used emergently to remove Cr (VI) from contaminated raw water sources due to sudden water pollution accidents [10]. Firstly, ferrous ion reduces Cr (VI) into Cr (III) at pH 2–3 [11]. Then, Cr (III) is precipitated into chromic hydroxide ($Cr(OH)_3$) at alkaline conditions and is removed by traditional coagulation, sedimentation, and filtration processes. Although reduction-precipitation with ferrous ions can effectively remove Cr (VI), it is difficult and expensive for a large-scale drinking water treatment plant to adjust the pH of raw water at a wide pH range from strong acidity to alkalinity. Furthermore, during the removal of Cr (VI) with ferrous ion, sludge containing chromium is generated and needs to be dealt with [12]. Activated carbon is also considered to be more favorable to cope with sudden Cr (VI) pollution because of its high specific surface area (BET) and pore volume [13]. At present, generally used commercial activated carbon is usually made of wood or coal [14,15]. This usually makes commercial activated carbon more expensive. Therefore, the development of low-price, green, and environment-friendly activated carbon using easily available materials that are carbon-rich has been a widely-held concern.

Sludge, a by-product generated from sewage treatment, can be used instead of coal or wood to produce activated carbon because of its rich organic matter [16]. This not only can lower the price of the prepared activated carbon but also can realize sludge resource utilization. At present, most sludge activated carbons are produced using urban sludge generated from urban sewage treatment plants [17]. The produced sludge activated carbons above have been applied as adsorbents removing Cr (VI) from industrial wastewater and have demonstrated a high removal efficacy for Cr (VI) [18,19]. However, few sludge activated carbons produced using urban sludge have been used in drinking water treatment because of the risk that heavy metal ions may be released from the sludge activated carbons into the drinking water [1]. Particularly, little attention has been focused on removing Cr (VI) from raw water sources contaminated by sudden water pollution accidents using sludge activated carbon as adsorbent. Therefore, we must seek out a type of sludge containing few heavy metal ions to produce activated carbon as a prospective adsorbent for the removal of Cr (VI) from contaminated raw water sources.

Cassava is widely grown worldwide and is used as raw material to produce fuel ethanol by fermentation [18]. Wastewater containing large amounts of organic matter is created in the process of producing fuel ethanol. Then, dewatered cassava sludge (DCS) is generated from wastewater treatment processes. As an organic industrial sludge, DCS has the advantages of being easy available, low-cost, and carbon-rich, and is a prospective raw material for the preparation of activated carbon. Furthermore, few heavy metals are involved in DCS. This makes it possible that activated carbon produced using DCS as a raw material can be applied to drinking water treatment to avoid the leakage of heavy metal ions. However, as far as we know, there have been few research reports on the preparation of activated carbon from DCS and the application of Cr (VI) removal in contaminated water sources.

Accordingly, we produced a new activated carbon (ACDCS), in which dewatered cassava sludge (DCS) and zinc chloride were used as raw materials and activators, respectively, and optimized the prepared process parameters in this study. Feasibility was investigated for the prepared ACDCS being used to remove Cr (VI) from a contaminated water source; the equilibrium, kinetics, and thermodynamics of Cr (VI) adsorbed on ACDCS were given; and the adsorption mechanisms of Cr (VI) on ACDCS were discussed.

2. Materials and Methods

2.1. Materials and Reagents

DCS collected from an alcohol plant in Taizhou, China, was first dried for 24 h at 378 K. All reagents comprising potassium dichromate ($K_2Cr_2O_7$), sodium hydroxide

(NaOH), hydrochloric acid (HCl), and Zinc chloride ($ZnCl_2$) were obtained from Sinopharm Chemical Reagent Co., Ltd., Shanghai, China. Only $ZnCl_2$ was of analytical reagent grade, and the other reagents were all in guaranteed grade.

2.2. Preparation Process of ACDCS and Parameters Optimization

The preparation of ACDCS was achieved by chemical activation using DCS as a raw material and zinc chloride ($ZnCl_2$) as an activator. The preparation process was as follows. A certain weight of DCS particles with different sizes (20–50, 50–100, 100–200, and >200 mesh) was immersed into a certain volume of $ZnCl_2$ solution with different concentrations (10%, 20%, 30%, 40%), subsequently activated at 333 K for a period (6, 12, 18, 24 h) in an Electro-thermostatic Water Cabinet (HWS24, Shanghai Yiheng Scientific Instrument Co., Ltd., Shanghai, China). Then, the activated DCS was pyrolyzed and carbonized in a muffle furnace (KSL-1200X, Hefei Kejing Material Technology Co., Ltd., Hefei, China) at the preset temperature (673, 773, 873, 973 K) for the desired retention time (30, 60, 90, 120 min). After cooling to room temperature, the obtained samples were fully pickled with 1.0 mol/L HCl solution, and then repeatedly rinsed with ultrapure water until turned neutral. After washing, the samples were dried, crushed, and ground into powder. The desired products were labeled as ACDCS, where (a) was DCS mesh, (b) was the activation time, (c) was the weight concentration of the $ZnCl_2$ solution, (d) was the carbonization temperature, and (e) was the carbonization time. For comparison, the unpretreated DCS, using Zinc chloride, produced sludge activated carbon according to a similar process as above, and the product was recorded as CDCS.

The orthogonal test method can optimize the process parameters of producing ACDCS by simplifying the multi-factor and multi-level experiment in this study. Based on literature and the preliminary experimental study, process parameters, including DCS particle size, activation time, weight concentration of $ZnCl_2$ solution, carbonization temperature, and carbonization time, play a key role in the performance of ACDCS. Consequently, the parameters above were chosen as factors, each factor was set at four value levels, and an $L_{16}(5^4)$ orthogonal table was designed. Furthermore, the value of iodine adsorbed on the prepared ACDCS (named as iodine value in this study) as a response, was used as an index for evaluating the performances of the prepared ACDCS.

2.3. Characterizations of ACDCS

The iodine number of ACDCS was determined according to the national standard testing method for wood activated carbon—Determination of iodine number (GB/T 12496.8-2015). The BET surface area and pore characteristics of ACDCS were measured by nitrogen adsorption using a specific surface area and porosity analyzer (ASAP 2460, Micrometrology, Norcross, USA) at 77K. The surface morphologies of the prepared ACDCS were evaluated using SEM (JSM-6490LV, Akishima-shi, Japan) to evaluate the ACDCS elemental constitution. The functional groups on the surface of each sample were analyzed before and after modification in the frequency range of 4000–400 cm^{-1} by Fourier transform infrared spectroscopy (Nicolet 6700, Nicolet, Madison, MI, USA). In addition, the zeta potentials of the ACDCS were analyzed by a Malvern Zetasizer Nano ZS90 (Malvern Instruments Ltd., Malvern, UK). X-ray photoelectron spectroscopy with the Al K-Alpha spectrometer (Axis Ultra DLD, Shimadzu-Kratos, Manchester, UK) was utilized to reveal the valence of elements and compositions of the samples' surface. The metal contents in leachate solution from the DCS and ACDCS were detected by an inductively coupled plasma-atomic emission spectrometer (ICP-AES, ThermoFisher, Waltham, MA, USA).

2.4. Adsorption Experiment

A definite amount of $K_2Cr_2O_7$ (2.829 g) was dissolved in 1 L ultrapure water to prepare Cr (VI) stock solution (1000 mg/L). Cr (VI) solutions with the desired concentration used as model water samples in this study were obtained by diluting stock solution. A certain amount of ACDCS was added into a series of Erlenmeyer flasks containing 500 mL of

Cr (VI) solution with the desired concentration. These flasks were sealed and shaken at 150 r/min for 180 min in a water bath shaker. After adsorption, the mixtures were filtered with 0.45 μm micro-membrane, and then the final concentration of Cr (VI) in each filtrate was determined using a UV-visible spectrophotometer at 540 nm. All the experiments were repeated three times.

The effects of adsorbent dosage (0.2–2.5 g), pH (2–13), contact time (0–180 min), and solution temperature (283–323 K) on Cr (VI) removal were investigated. Kinetics studies were carried out by varying initial Cr (VI) concentrations (1, 5, 10 mg/L), and a water sample was drawn at regular time intervals for the concentration of Cr (VI) measurements. Isotherm experiments were carried out at three temperatures (283, 293, 303 K) using varying initial Cr (VI) concentrations (1–15 mg/L). The removal percentage of Cr (VI), E (%), and the amount of Cr (VI) adsorbed on adsorbent at time t, q_t was calculated by using the following expressions:

$$R(\%) = (C_0 - C_t)/C_0 \times 100\% \quad (1)$$

$$q_t = (C_0 - C_t) \times V/W \quad (2)$$

where C_0 and C_t (mg/L) are the initial concentration and the final concentration of Cr (VI) at contact time t (min), respectively; R (%) is the removal efficiency of Cr (VI); q_t (mg/L) is the adsorption capacity and at time t (min); W (g) is the weight of ACDCS; and V (L) is the volume of Cr (VI) solution.

3. Results and Discussion

3.1. Optimization of Preparation Parameters of ACDCS

The preparation conditions of ACDCS were optimized by 16 groups of orthogonal experiments, and the results are shown in the supplementary material (demonstrated in Table S1). The iodine values of the prepared ACDCS varied from 274.52 mg/g to 557.10 mg/g at various preparation conditions. The results showed that the different preparation parameters had a considerable influence on the adsorption performances of the prepared ACDCS.

The R value (response at the average of the difference between the extreme values of Ki) can be applied to evaluate the significance of the influence of various factors on the performance of the prepared ACDCS, and the larger the R value, the more considerable the influence of the factor [20]. Based on the viewpoint above, the impact degree of the selected factors in this study was in the order DCS particle size > carbonization temperature > $ZnCl_2$ weight concentration > activation time > carbonization time. In addition, it was found that the R values of the DCS particle size and carbonization temperature were much higher than those of the other three factors. This indicated that sludge size and carbonization temperature were the key factors affecting the performances of the prepared ACDCS. DCS particle size had the greatest impact on the iodine value. This was because the contents of organic matter and ash varied remarkably for different-sized DCS sludge particles (demonstrated in Table S2). For raw materials used to produce activated carbon, a high content of organic matter and low ash content could significantly improve the adsorption properties of prepared activated carbon [21]. Accordingly, the organic matter content of the raw material was a key factor for producing high-quality activated carbon. Furthermore, carbonization temperature was another crucial parameter for influencing the properties of ACDCS. This was because the carbonization temperature affected the pyrolysis reaction process of sludge and $ZnCl_2$, thereby improving or decreasing the pore structure of the prepared ACDCS [22].

For a factor, the K_i value (sum response at the ith level) can be applied to recognize the optimal level, and the maximum value of K_i denotes the optimal level [23]. Based on the theory above, the optimal preparation conditions for ACDCS in this study are as follows: DCS particle size 20–50 mesh, $ZnCl_2$ weight concentration 20%, activation time 12 h, carbonization temperature 773 K, and carbonization time 60 min. The iodine number adsorbed on the prepared ACDCS at the optimal process parameters added to 557.10 mg/g,

in contrast to other adsorbents [22,24,25]. The prepared ACDCS at the optimal conditions was applied to the subsequent adsorption experiments and was recorded as $ACDCS_{optimal}$.

3.2. Effect of $ACDCS_{optimal}$ Dosage

The effects of the dosage of DCS (dewatered cassava sludge), CDCS (carbonized dewatered cassava sludge without activation), and $ACDCS_{optimal}$ on the removal of Cr (VI) were studied, and the results are presented in Figure 1A. Compared with DCS and CDCS, the removal efficacy of Cr (VI) adsorbed on $ACDCS_{optimal}$ was much better at the same dosage. The SEM images of DCS, CDCS, and $ACDCS_{optimal}$ can be found in the supplementary material (demonstrated in Figure S2). The surface of DCS was smooth without obvious pores. Although a few folds appeared on the surface of the CDCS, the surface was poor in the pore structure. However, the surface of the $ACDCS_{optimal}$ was rich in pore structure, resulting in much larger specific surface areas (509.03 m^2/g, shown in Table S2) compared with DCS and CDCS. This could be the reason for causing the better removal of the Cr (VI) adsorbed on $ACDCS_{optimal}$. Moreover, this indicates that activation with a proper activator ($ZnCl_2$) during the process of producing activated carbon can obviously elevate the performance of prepared activated carbon [26].

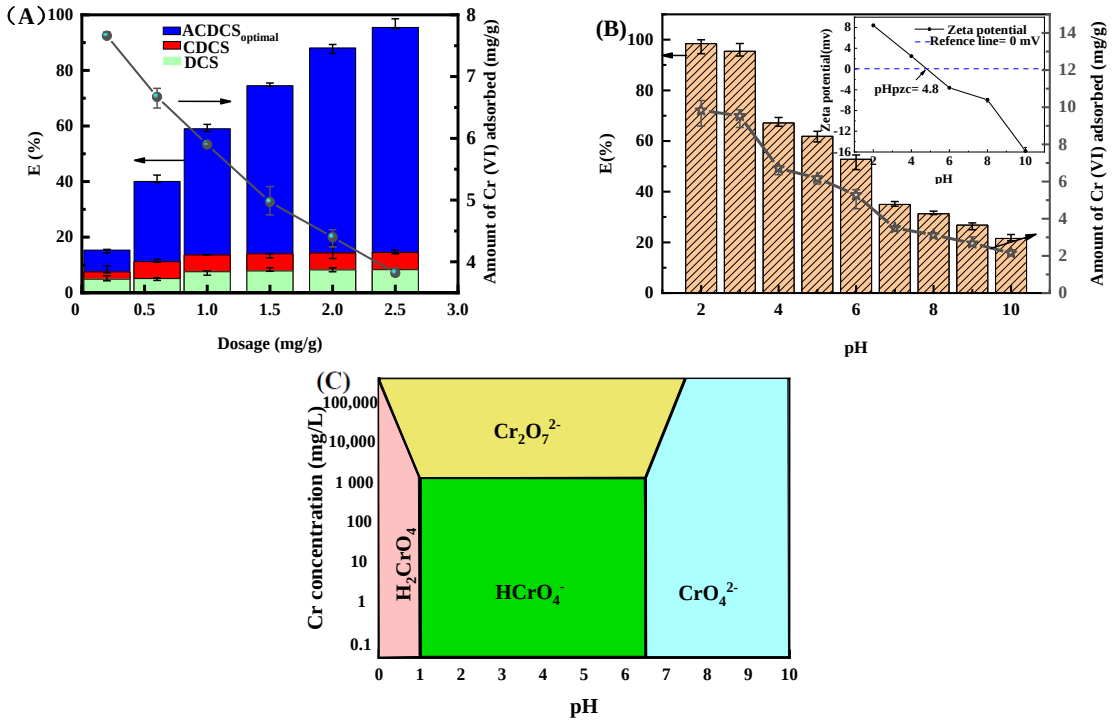


Figure 1. Effect of adsorbent dosage (**A**) (Cr (VI) concentration: 10 mg/L; pH: 6.2 ± 0.1; adsorption time: 3 h; temperature: 293 K); effect of pH (**B**) (initial Cr (VI) concentration: 10 mg/L; dosage: 1 g/L; adsorption time: 3 h; temperature: 293 K); relative distribution of Cr (VI) species in water (**C**).

As shown in Figure 1A, the removal efficiency of Cr (VI) rapidly increased from 15.32% to 95.44% with an increasing dosage of $ACDCS_{optimal}$ from 0.2 to 2.5 g/L. This was because the adsorption sites available increased with the increasing adsorbent dosage. Nevertheless, the amount of Cr (VI) adsorbed on $ACDCS_{optimal}$ declined from 7.66 to 3.82 mg/g with the increasing adsorbent dosage. This was attributed to the overlapping of active sites at high dosage, causing a decrease in effective contact surface [27]. In addition, at a high dosage, the excessive active sites were not utilized effectively for a certain Cr (VI). This may be another reason causing the decrease in the amount of Cr (VI) adsorbed on $ACDCS_{optimal}$ with an increase in the adsorbent dosage. Accordingly, the prepared $ACDCS_{optimal}$ at the

optimal level was applied in subsequent tests, and the dosage of $ACDCS_{optimal}$ was 1.0 g/L in this study, unless otherwise stated.

3.3. Effect of pH

The pH value of the solution, affecting the surface properties of the adsorbent and the chemical form of the adsorbate, is an important parameter of the adsorption process [28]. Figure 1B shows the relationship between the solution's pH and the removal efficiency of Cr (VI) adsorbed on $ACDCS_{optimal}$. The maximum amount of Cr (VI) adsorbed on $ACDCS_{optimal}$ was found to be 9.84 mg/g, and the removal efficiency of Cr (VI) was 98.43% at pH 2.0. The amount of Cr (VI) adsorbed dwindled from 9.84 mg/g to 0.15 mg/g with the increase in pH from 2.0–10.0. This result suggests the adsorption removal of Cr (VI) is a highly pH-dependent process.

Depending on the pH of the solution and the Cr (VI) concentration, Cr (VI) exists in different forms (H_2CrO_4, $HCrO_4^-$, CrO_4^{2-}, $Cr_2O_7^{2-}$) (shown in Figure 1C) in aqueous solution [29]. Moreover, the surface charge of $ACDCS_{optimal}$ (given in Figure 1B) was affected by aqueous solution pH as well [28]. The pH at the point of zero charges (pH_{pzc}) for $ACDCS_{optimal}$ was found to be 4.8, indicating that the surface of $ACDCS_{optimal}$ was charged positively at pH < 4.8 and, conversely, the surface of $ACDCS_{optimal}$ showed a negative charge at pH > 4.8. At pH = 2, Cr (VI) mainly exists in the anion form of $HCrO_4^-$. The surface of $ACDCS_{optimal}$ was loaded with a lot of positive charges due to the protonation, and the strong electrostatic attraction between the positively charged surface of $ACDCS_{optimal}$ and the negatively charged anion $HCrO_4^-$ achieved the highest removal of Cr (VI) at pH = 2.0. The electrostatic attraction decreased gradually due to the fade of the protonation with the increase in pH from 2 to 4.8, leading to a decline in the removal of Cr (VI). After pH > 4.8, the surface of the $ACDCS_{optimal}$ was charged negatively, and the electrostatic attraction between $ACDCS_{optimal}$ and $HCrO_4^-$ vanished. The reduction of Cr (VI) to Cr (III), and the ion exchange of Cr (III) with adsorption sites at acidic conditions, might play key roles in the removal of Cr (VI) [30]. With an increase in pH from 4.8 to 7.0, the reduction and ion exchange were weakened gradually, resulting in a decline in the removal of Cr (VI). After pH > 7.0, the van der Waals forces probably contributed to $ACDCS_{optimal}$ adsorption of Cr (VI) removal because of the vanishing of the reduction and electrostatic attraction [31]. CrO_4^{2-} ions were confirmed as the dominant species of Cr (VI) in an aqueous solution at pH > 7.0 (seen in Figure 1C). In comparison with $HCrO_4^-$, the stronger repulsion forces between the surface of $ACDCS_{optimal}$ and CrO_4^{2-} ions decreased the removal of Cr (VI) with the increase in pH from 7.0 to 10.0 [32]. Furthermore, the competition between the excess OH^- and CrO_4^{2-} for the adsorption sites might be another reason causing the decline in the Cr (VI) removal with the increase in pH from 7.0 to 10.0 [31].

3.4. Adsorption Kinetics

3.4.1. Effect of Initial Cr (VI) Concentration and Adsorption Time

Adsorbate concentration and adsorption time are significant parameters for developing cost-effective adsorption procedures [33]. Figure 2A shows the relationship of the amount of Cr (VI) adsorbed on $ACDCS_{optimal}$ and adsorption time at different initial Cr (VI) concentrations.

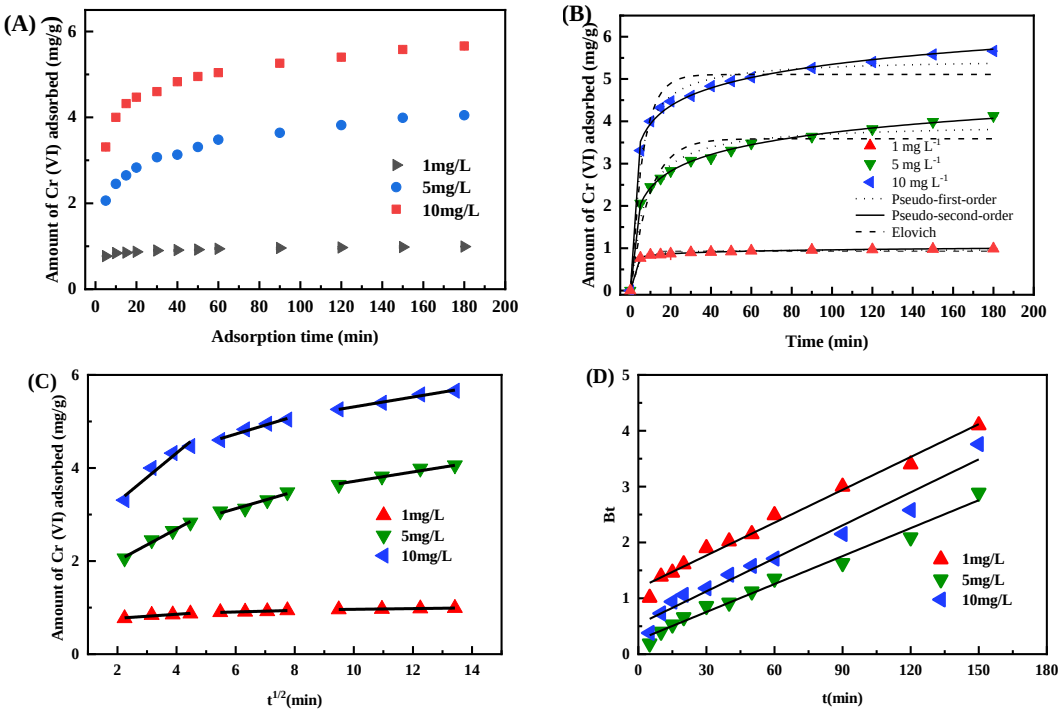


Figure 2. Effect of the relationship between initial concentration on Cr (VI) and adsorption time (**A**); Kinetic fitting curve of Cr (VI) adsorption on $ACDCS_{optimal}$ (**B**); Weber-Morris diffusion model fitting curve (**C**); Boyd diffusion model fitting curve (**D**). (pH = 6.2 ± 0.1; dosage: 1 g/L; temperature: 293 K).

It can be easily observed that the adsorption process of Cr (VI) on $ACDCS_{optimal}$ included three stages: rapid adsorption (0–20 min), slow adsorption (20–150 min), and reaching adsorption equilibrium (180 min). In the initial stage of adsorption, the rapid removal of Cr(VI) was because there were more vacancies on the $ACDCS_{optimal}$ surface; and, because the concentration gradient between the bulk solution and the $ACDCS_{optimal}$ surface was larger, the driving force was higher. [34]. However, with the continuous decrease of the density of vacant active centers, the adsorption rate gradually slowed down [35]. At nearly 180 min, the amount of Cr (VI) adsorbed showed no obvious change, indicating that equilibrium was achieved [33].

Moreover, It was also observed that as the initial concentration of Cr(VI) increased from 1.0 mg/L to 10 mg/L, the amount of Cr (VI) adsorbed increased. The active adsorption sites, including the external surface sites and the internal pore sites, were fixed at the $ACDCS_{optimal}$ dosage of 1 g/L in this study. At a low Cr (VI) concentration (for example, 1.0 mg/L), the active sites of $ACDCS_{optimal}$ were sufficient for the contents of Cr (VI), and all the Cr (VI) ions were almost adsorbed by the external surface sites. As the initial Cr (VI) concentration gradually increased, the external surface active sites of $ACDCS_{optimal}$ were completely occupied, and the higher Cr (VI) concentration gradient promoted the continued diffusion of the Cr (VI) ions into the internal pore sites [27]. The sufficient utilization of active sites of $ACDCS_{optimal}$ might be the reason causing the increase in the amount of Cr (VI) adsorbed with the increase in the initial concentration of Cr (VI) solution [33]. Moreover, Figure 2A demonstrates that the initial concentration of Cr (VI) solution was directly proportional to the time required to reach equilibrium. Compared with the internal pore adsorption at the higher Cr (VI) concentration, the external surface adsorption was much faster at the low Cr (VI) concentration. This could be because as the initial concentration of Cr(VI) increased, it needed to take longer to reach equilibrium.

3.4.2. Kinetics Models

Adsorption kinetics is of major significance for the study of reaction pathways and mechanisms [36]. In order to investigate the adsorption kinetics of Cr (VI) on $ACDCS_{optimal}$,

the pseudo-first-order model (PFO), pseudo-second-order model (PSO), and Elovich model were used employed to describe the adsorption process of Cr (VI) on $ACDCS_{optimal}$ in this work [37], and they were expressed by Equations (3)–(5):

$$q_t = q_e[1 - \exp(-k_1 t)] \quad (3)$$

$$q_t = k_2 q_e^2 t / (1 + k_2 q_e t) \quad (4)$$

$$q_t = \beta^{-1} \ln(1 + \alpha\beta t) \quad (5)$$

where q_t (mg/g) is the adsorption capacity at time t; k_1 and k_2 (mg/(g min)) are the equilibrium rate constants of the PFO model and the PSO model, respectively; q_e represents the equilibrium adsorption capacity; α is the original adsorption rate constant (mg/(g min)); and β is concerned with the extent of surface coverage and activation energy for chemisorption (mg/g).

The relevant parameters of the three kinetic models with the correlation coefficients at diverse initial solution concentrations of Cr (VI) are presented in Table 1 and Figure 2B. The results showed that the correlation coefficients (R^2) of the Elovich model were larger than those of the PFO model and PSO model, and the SEE values of the Elovich model were the smallest among the three models. This indicated that the Elovich was the best representation for adsorption of Cr (VI) on $ACDCS_{optimal}$. Further, adsorption of Cr (VI) on $ACDCS_{optimal}$ might be chemisorption by transferring electrons [37].

Table 1. The kinetic parameters at different initial Cr (VI) concentrations.

Models and Parameters	1 mg/L	5 mg/L	10mg/L
q_{eexp}	0.99	4.13	5.66
Pseudo-first-order model			
q_{ecal} (mg/g)	0.93	3.59	5.11
k_1 (mg/(g·min))	0.3189	0.1049	0.1609
R_2	0.4939	0.6580	0.6855
SSE	0.02216	1.39233	1.37441
Pseudo-second-order model			
q_{ecal} (mg/g)	0.97	3.95	5.49
k_2 (mg/(g·min))	0.6849	0.0384	0.0469
R^2	0.8761	0.8901	0.9282
SSE	0.00542	0.44748	0.29537
Elovich model			
α (mg/(g·min))	8072.6012	3.9535	39.0889
β (g/mg)	17.084	1.7504	1.6394
R^2	0.9844	0.9960	0.9823
SSE	6.83×10^{-4}	0.01627	0.1229
Weber-Morris model			
k_{id1} (mg/(g·min$^{0.5}$))	0.0431	0.3424	0.5247
C_1 (mg/g)	0.6846	1.3215	2.2228
R^2	0.8553	0.9841	0.9322
k_{id2} (mg/(g·min$^{0.5}$))	0.0170	0.1845	0.1920
C_2 (mg/g)	0.8042	2.0196	3.5770
R^2	0.9225	0.9162	0.9548
K_{id3} (mg/(g·min$^{0.5}$))	0.0076	0.1011	0.1057
C_3 (mg/g)	0.8871	2.7024	4.2572
R^2	0.9963	0.9263	0.9808
Boyd model			
R^2	0.9833	0.9624	0.9809

3.4.3. Diffusion Mechanism

Although the adsorption process of Cr (VI) on $ACDCS_{optimal}$ was fitted well by the Elovich kinetic model, it still could not confirm the diffusion mechanism and the rate-controlling step in the adsorption process, such as film diffusion and intra-particle diffusion. To identify the step of actual rate-controlling in the adsorption process for Cr (VI), the Weber-Morris model was used [38].

$$q_t = k_{id} t^{0.5} + C_i \quad (6)$$

where q_t (mg/g) is the amount of Cr (VI) adsorbed at time t (min), k_{id} is the intra-particle diffusion rate (mg/(g $min^{0.5}$)), and C_i represents the diffusion effects of the boundary layer. Based on the Weber-Morris model, the fitting result of q_t to $t^{0.5}$ is linear, and the line passes through the origin if the intra-particle diffusion process is a rate-determining step. Otherwise, the adsorption process could be affected by more steps [39].

The fitted plots of q_t against $t^{0.5}$ at different initial Cr (VI) concentrations are shown in Figure 2C, and the parameters of k_{id} and C_i were calculated according to the model and are listed in Table 1. Obviously, the adsorption data were fitted very well by the three straight lines, suggesting that three stages occurred during Cr (VI) adsorption on $ACDCS_{optimal}$ [40]. Firstly, the linear section had a higher slope, indicating that Cr (VI) was transferred to the external surface of $ACDCS_{optimal}$ from an aqueous solution [38]. Then, the slope of the straight section decreased gradually, suggesting that Cr (VI) diffused from the external into the interior pore structure of $ACDCS_{optimal}$ [27]. Finally, the slope of the straight section approached zero, indicating that the adsorption equilibrium was reached [40]. In addition, the values of C_i at all the stages were greater than zero, indicating that the process was not only intra-particle diffusion but also some other steps that might control the rate of the kinetic process [38]. Further, the Boyd model (given in Equation (7)) was used to check whether the film diffusion was involved in the adsorption process, and the results are represented in Figure 2D and Table 1, respectively.

$$Bt = -0.4977 - \ln\left(1 - \frac{q_t}{q_e}\right) \quad (7)$$

where Bt is the time constant; q_t (mg/g) is the amount of Cr (VI) adsorbed at time t (min); and q_e is the equilibrium adsorption capacity. Based on the Boyd model, the fitting result of B to t^{-1} is not linear, or the linear does not pass through the origin of the film diffusion process, which is a rate-determining step [39].

It was found that the plots fitted by the Boyd model demonstrated good linearity with a high R^2 value (0.9833, 0.9624, 0.9809), and the fitting lines were the extended model and did not pass through the origin at different initial Cr (VI) concentrations. Those results confirmed that film diffusion occurred during the adsorption process of Cr (VI) on $ACDCS_{optimal}$ [39]. To sum up, the adsorption process of Cr (VI) on $ACDCS_{optimal}$ was mainly affected and controlled by film diffusion and intra-particle diffusion. Firstly, Cr (VI) ions diffused from the bulk solution to the external surface of $ACDCS_{optimal}$, and this process was controlled by film diffusion. Then, the next process was dominated by intra-particle diffusion, in which Cr (VI) ions entered the internal pores to load into the internal active adsorption sites until adsorption equilibrium.

3.5. Adsorption Equilibrium

3.5.1. Effect of Temperature

In a solid-liquid adsorption system, solution temperature plays a key role [36]. The equilibrium tests of Cr (VI) adsorbed on $ACDCS_{optimal}$ were investigated at 283, 293, and 303 K, and the results are shown in Figure 3A. It was observed that the equilibrium adsorption capacity of Cr (VI) on $ACDCS_{optimal}$ increased slightly with the increase in solution temperature from 283 to 303 K, indicating that the increasing temperature of the solution was conducive to the adsorption removal of Cr (VI). This was because the

increase of temperature promoted the thermal movement of Cr (VI) ions in the solution and facilitated the diffusion of Cr (VI) ions into the internal active adsorption sites of $ACDCS_{optimal}$ [27].

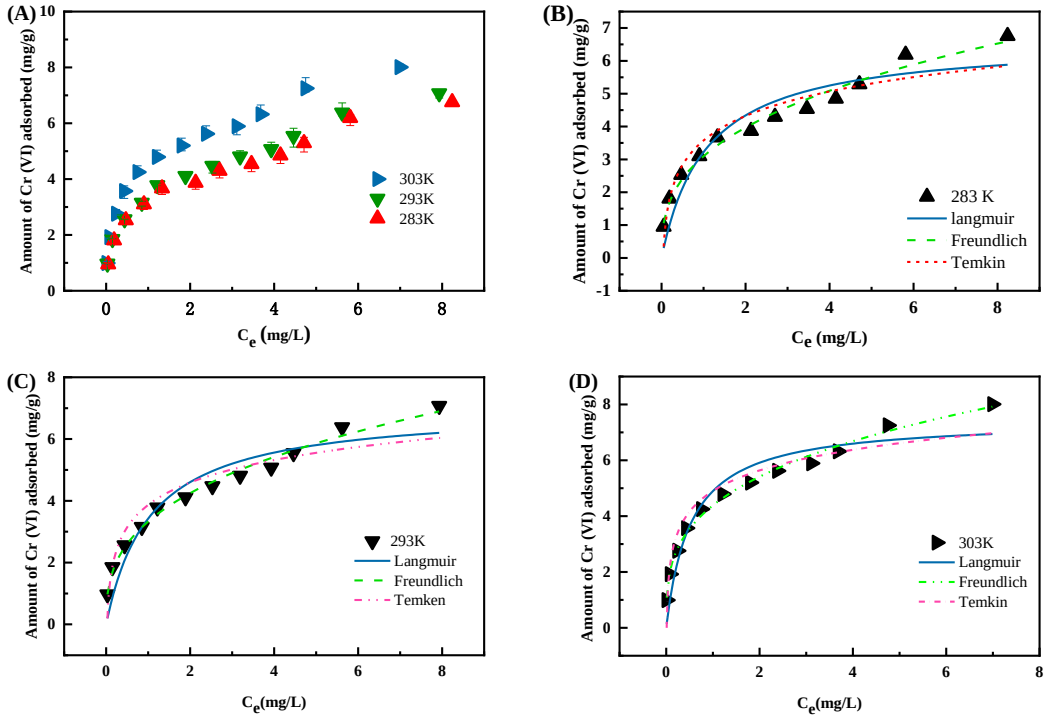


Figure 3. Effects of temperatures (**A**); isotherm fitting diagram of Cr (VI) adsorption on $ACDCS_{optimal}$ at different temperatures for (**B**–**D**) (pH = 4.0 ± 0.1; dosage: 1.0 g/L).

3.5.2. Adsorption Isotherm Models

The adsorption isotherm showed a specific relationship between its accumulation on the surface of the adsorbent and the concentration of adsorbate [39]. Three isotherm models were used to fit the equilibrium experimental data of Cr (VI) on $ACDCS_{optimal}$. These isotherm models included the Langmuir model, Freundlich model, and Temkin, and they were expressed by Equations (8)–(10) [41]. The fitted curves and model parameters with R^2 are presented in Figure 3B–D and Table 2, respectively.

$$q_e = (q_m K_L C_e)/(1 + K_L C_e) \quad (8)$$

$$q_e = K_F C_e^{\frac{1}{n}} \quad (9)$$

$$q_e = B_T \ln(A_T C_e) \quad (10)$$

where q_e is the equilibrium adsorption capacity; q_m is the maximum single-layer adsorption capacity of the adsorbent; K_L is the Langmuir constant; Ce is the equilibrium concentration of Cr (VI) solution; K_F is the Freundlich adsorption constant; n is the adsorption strength; B_T is the heat of adsorption; and A_T is the equilibrium constant.

Table 2. Fitting results of adsorption isotherm model of Cr (VI).

Models and Parameters	283 K	293 K	303 K
q_{eexp}	6.76	7.07	8.01
Langmuir model			
q_m (mg/g)	6.6368	7.0219	7.4593
K_L (L/mg)	0.9441	0.9524	1.9104
R_L	0.5143–0.0659	0.5121–0.06542	0.3436–0.03372
R^2	0.88	0.89	0.90
Freundlich model			
K_F ((mg/g)/(mg/L)$^{1/n}$)	3.0958	3.3290	4.3829
1/n	0.3587	0.3515	0.3044
R^2	0.98	0.99	0.99
Temkin model			
A_T (L/g)	27.6142	40.1145	100.0136
B_T (J/mol)	2.3527	2.436	2.5191
R^2	0.91	0.90	0.92
Dubinin-Radushkevich model			
q_{max} (mg/g)	6.210	6.628	7.678
K_{dr} (mol^2/J^2)	5.0555×10^{-8}	4.5033×10^{-8}	2.5372×10^{-8}
E (kJ/mol)	3.14	3.33	4.44
R^2	0.87	0.87	0.93

It was evident that the Freundlich isotherm model showed a better fitting to the equilibrium adsorption data in terms of the coefficient of determination ($R^2 > 0.98$). The Freundlich isotherm model is suitable for highly heterogeneous surfaces, and the lack of a saturated platform for Freundlich isotherm may indicate a multilayer adsorption mechanism [39]. Based on this viewpoint, the adsorption process of Cr (VI) on $ACDCS_{optimal}$ was a multilayer adsorption process over a heterogeneous surface. Moreover, the parameter n was very important for the Freundlich isotherm model. The adsorption type is considered favorable when n is more than 1.0, and the adsorption process occurs very easily when n^{-1} is less than 0.5. The fitted results confirmed the adsorption process of Cr (VI) on $ACDCS_{optimal}$ was very easy to carry out.

3.6. Energy Changes during the Adsorption Process

3.6.1. Adsorption Thermodynamics

Adsorption thermodynamics can reflect the energy changes during the process of target pollutants adsorbed on the adsorbent, and can be used to analyze and explain the adsorption mechanism from the perspective of thermodynamics [25]. The thermodynamic parameters of the adsorption of Cr (VI) onto $ACDCS_{optimal}$, including the Gibbs free energy change (ΔG°, kJ/mol), changes of adsorption heat (ΔH°, kJ/mol), and changes of adsorption entropy (ΔS°, J/mol/K), were determined by the van't Hoff approach using Equations (11)–(13) [29]:

$$K_D = \frac{C_0 - C_t}{C_t} \times \frac{V}{M} \tag{11}$$

$$\ln K_D = \frac{\Delta S^\circ}{R} - \frac{\Delta H^\circ}{RT} \tag{12}$$

$$\Delta G^\circ = \Delta H^\circ - T\Delta S^\circ \tag{13}$$

where C_0 and C_t (mg/L) are the initial concentration and the final concentration of Cr (VI) at contact time t (min), respectively; R (8.314 J/(mol·K)) is the universal gas constant; T (K) is the absolute temperature; W (g) is the weight of ACDCS; V (L) is the volume of Cr (VI) solution; and K_D (L/g) is the distribution coefficient of Cr (VI) in $ACDCS_{optimal}$ and solution.

The plot of ln (K_D) against 1/T is shown in Figure S1. The parameters of ΔH° and ΔS° were determined through the slope and intercept value, respectively. The calculated values of ΔH°, ΔS°, and ΔG° for the adsorption of Cr (VI) on $ACDCS_{optimal}$ are given in Table 3.

Table 3. Adsorption thermodynamic parameters of Cr (VI).

T (K)	ΔG° (kJ/mol)	ΔS° (J/mol/K)	ΔH° (kJ/mol)
283	−10.43		
293	−10.80		
303	−11.16	36.88	10.13
313	−11.53		
323	−11.90		

The negative ΔG° indicates that the process of Cr (VI) adsorbed on $ACDCS_{optimal}$ was spontaneous. The positive values of ΔS° indicate that the adsorption process is entropy-driven rather than enthalpy. Furthermore, the positive ΔH° confirms the endothermic nature, and that the increasing temperature favored the adsorption process. Moreover, the values of ΔG° indicate the physical or chemical nature of adsorption [25]. The values of ΔG° were <−10 kJ/mol in this study, implying that physisorption was one of the mechanisms for the removal of Cr (VI) adsorbed on $ACDCS_{optimal}$.

3.6.2. Average Free Energy

The calculation of average free energy is a method based on the fitting analysis of the Dubinin-Radushkevich (D-R) isotherm model to determine the reaction type [42]. The isotherm model and the average free energy calculation formula were as follows:

$$q_e = q_{max} \exp\left(-K_{dr}\varepsilon^2\right) = RT\ \ln(1 + 1/C_e) \quad (14)$$

$$E = (2K_{dr})^{-0.5} \quad (15)$$

where q_{max} is the maximum adsorption capacity of Cr (VI); q_e is the equilibrium adsorption capacity; R (8.314 J/(mol·K)) is the universal gas constant; T (K) is the absolute temperature; Ce is the equilibrium concentration of Cr (VI) solution; K_{dr} (mol^2/J^2) is a model parameter related to the average adsorption energy; and E is the average free energy.

The fitted results and model parameters with R^2 are presented in Table 2. It was evident that the Dubinin-Radushkevich isotherm model showed a good fitting to the equilibrium data in terms of coefficients of determination ($R^2 > 0.87$). The average free energy (AFE) for the adsorption of Cr (VI) on $ACDCS_{optimal}$ at 283 K, 293 K, and 303 K were 3.14 kJ/mol, 3.33 kJ/mol, and 4.44 kJ/mol, respectively. The values of AFE were less than 8 kJ/mol at a different temperature, indicating that the physisorption occurred during the process of Cr (VI) adsorbed on $ACDCS_{optimal}$ [43].

3.6.3. Adsorption Activation Energy

The activation energy can be used to judge the difficulty of the adsorption process [31]. The Arrhenius equation was used to calculate the adsorption activation energy, expressed by Equations (13):

$$\ln k = \ln A - E_a/RT \quad (16)$$

where E_a is adsorption activation energy (kJ/mol); A is frequency factor; R is the gas constant (8.314 J/(mol·K)); T (K) is the absolute temperature; and k is the reaction rate constant.

The data of ln k versus 1/T were plotted and are shown in Figure S1. The correlation coefficient (R^2 = 0.97) showed that there was a good linear relationship between a value and 1/T. The weak van der Waals force is the cause of physical adsorption, and its activation energy is lower than 4.18 kJ/mol [31]. In this study, the value of E_a was 3.37 kJ/mol,

indicating that the adsorption process of Cr (VI) on $ACDCS_{optimal}$ was easy to carry out and that physical adsorption was involved.

3.7. Adsorption Mechanism

3.7.1. Pore Filling

The excellent adsorption performances of carbon material are based on its developed pore structure and high specific surface areas, resulting in the fact that pore filling is the most basic adsorption mechanism in the removal of pollutants [28]. The prepared fresh $ACDCS_{optimal}$ in this study possessed rich pores, and the total pore volume added to 0.375 cm^3/g (demonstrated in Table S2). Furthermore, Table S2 demonstrates that the pore sizes were mainly distributed in the range around the micropores and mesopores, leading to a high BET surface area (509.03 m^2/g). This was favorable for the removal of Cr (VI) adsorbed on $ACDCS_{optimal}$. In addition, the surface pores were covered after adsorption, showing that Cr (VI) ions were adsorbed on the pores (demonstrated in Table S2 and Figure S2). The Cr (VI) ions could diffuse into the internal pores due to the smaller size, compared with the sizes of micropores and mesopores [28]. The decreased BET surface areas and total pore volume (demonstrated in Table S2) after adsorption indicate that the Cr (VI) ions were removed on the internal active sites. The results above confirm that pore filling was one of the mechanisms for the removal of Cr (VI) adsorbed on $ACDCS_{optimal}$.

3.7.2. Electrostatic Attraction

As discussed in Section 3.3, the $ACDCS_{optimal}$ exhibited a positively charged surface resulting from the $–OH_2^+$ functional groups because of the protonation at pH < 4.8. In addition, Cr (VI) mainly existed in the form of $HCrO_4^-$ ion. The strong electrostatic attraction was formed between $–OH_2^+$ and $HCrO_4^-$, facilitating the removal of Cr (VI). The electrostatic attraction disappeared after pH > 4.8 due to the $ACDCS_{optimal}$ surface having negative charges, although Cr (VI) still appeared in the anions ($HCrO_4^-$ or CrO_4^{2-}).

3.7.3. Adsorption-Combined Reduction

The Cr (VI) adsorbed on $ACDCS_{optimal}$ might be reduced by the functional groups on the carbon surface at the acidic conditions (shown in Equation (14)). Compared with the fresh $ACDCS_{optimal}$, two new peaks at 576.51 eV and 585.88 eV, attributed to $Cr2p_{3/2}$ and $Cr2p_{1/2}$, respectively, were found in the XPS wide spectra of $ACDCS_{optimal}$ after adsorption (demonstrated in Figure S3). This indicated chromium was adsorbed on $ACDCS_{optimal}$ [27]. The two peaks at 579.17 eV and 587.60 eV were ascribed to Cr (VI), and the peaks at 585.88 eV and 576.51 eV were considered as Cr (III) in the high-resolution spectrum of Cr2p [32]. Those results confirmed that the Cr (VI) adsorbed on the $ACDCS_{optimal}$ was partially reduced to Cr (III) by the rich functional groups on the surface of $ACDCS_{optimal}$, such as the –OH and C–H groups (shown in Equations (15) and (16)) [39].

In comparison, the atomic ratio of graphitic carbon after adsorption (C–C and/or C–H) was decreased to 73.88%, and the contents of the C=O and C–O bond increased to 7.58% and 18.53%, respectively [27]. This showed that some graphitic carbon was oxidized by Cr (VI) (shown in Equations (15) and (16)) [39]. The existence of chemical coordination between Cr (VI) and the C–O functional groups was due to a slight shift at the energy of 285.95 eV.

The FTIR spectra of $ACDCS_{optimal}$ before and after adsorption was also used to analyze the functional groups involved in the redox reaction. The peak, at approximately 3428 cm^{-1}, was associated with the –OH functional groups, and the peak slightly shifted because of Cr (VI) adsorbed. Furthermore, the peaks at 2923 and 2857 cm^{-1} slightly decreased because of –C–H stretching [25]. These results indicate that the –OH functional groups and graphitic carbon (–C–H) were oxidized because of the reduction of Cr (VI) to Cr (III) [44]. Further, the peak at 1617 cm^{-1} shifted to 1565 cm^{-1}, which could be associated with stretching vibrations of $–COO^-$ [35]. These results suggest that the carboxyl functional groups increased after Cr (VI) removal, and chromium was chemically immobilized on

these oxygen-containing groups [39]. Hence, Cr (III), as a reductive product of Cr (VI), was removed by ion exchange with the –COOH functional groups as well pore filling. The characterizations of the above studies are presented in the form of Supplementary Materials (demonstrated in Figure S3).

$$HCrO_4^- + 7H^+ + 3e^- \rightarrow Cr^{3+} + 4H_2O \quad (17)$$

$$-C-H + Cr(VI) + H_2O \rightarrow -C-OH + Cr(III) + H^+ \quad (18)$$

$$-C-OH + Cr(VI) + H_2 \rightarrow COOH + Cr(III) + H^+ \quad (19)$$

Based on the discussion above, the removal of Cr (VI) with $ACDCS_{optimal}$ was dependent on the pH of the solution, and the mechanism was considered to comprise the following three sections, as illustrated in Figure S4: (i) the reduction reaction and ion exchange were involved in the removal of Cr (VI), as well pore filling and electrostatic attraction at pH < 4.8; (ii) pH = 6.5, with the electrostatic attraction disappearing due to deprotonation of the oxygen-containing groups, pore filling, reduction reaction, and ion exchange, contributed to the removal of Cr (VI) at 4.8 < pH < 6.5; (iii) pore filling played the main role for the removal of Cr (VI) on $ACDCS_{optimal}$ at the alkaline conditions.

3.8. Comparison with Other Adsorbents for Cr (VI)

Although it is difficult to compare with various adsorbents due to different test conditions, the maximum adsorption capacity (q_{max}) is still used as a parameter for comparison. The results in the literature are listed in Table 4. Table 4 demonstrates that it was comparable for the prepared $ACDCS_{optimal}$ in this study with the shorter adsorption time and the higher maximum adsorption capacity. In addition, the trace metal leakage (demonstrated in Table S3) indicated that the prepared $ACDCS_{optimal}$ was a potential adsorbent for the removal of Cr (VI) from the contaminated raw water.

Table 4. Comparison with various sludge activated carbons.

Adsorbents	Adsorption Time	q_{max} (mg/g)	Dosage (g/L)	pH	Reference
Paper mill sludge	3.0 h	23.18	3.5	4.0	[45]
Sludge derived biochar	16.0 h	16.18	1.0	5.0	[46]
Anaerobic granular sludge	2.5 h	13.19	1.5	4.5	[47]
Sewage sludge	24 h	11.56	4.0	2.0	[48]
$ACDCS_{optimal}$	3.0 h	9.84	1.0	2.0	This study
Peanut shell	16.0 h	8.31	2.5	2.0	[29]
Municipal sludge	8.0 h	7.0	1.25	2.0	[17]
Biochars	12.0 h	6.08	2.0	1.75	[49]
Distillery sludge	2.0 h	5.7	5.0	3.0	[50]
Oak wood	48.0 h	5.50	10	2.0	[51]

4. Conclusions

A novel sludge activated carbon was produced successfully by pyrolysis using dewatered cassava sludge as the raw material and $ZnCl_2$ as the activator. The removal performances and mechanisms of Cr (VI) on the prepared sludge activated carbon were systemically investigated. The optimal preparation parameters were as follows: DCS particle size 20–50 mesh, $ZnCl_2$ weight concentration 20%, activation time 12 h, carbonization temperature 773 K, and carbonization time 60 min. The specific surface areas and iodine value for the prepared sludge activated carbon (named as $ACDCS_{optimal}$) at the optimal process parameters added to 509.03 m^2/g and 557.10 mg/g, respectively. The initial Cr (VI) concentration affected the time of reading equilibrium, but the adsorption could be fulfilled within 3 h. The kinetics could be fitted well by the Elovich model. The whole adsorption rate was controlled by both film and intra-particle diffusion. The adsorption equilibrium could be described well by the Freundlich isotherm model. The maximum equilibrium

capacity was 8.01 mg/g. The adsorption was a spontaneous and endothermic process. Elevating temperature facilitated the removal of Cr (VI) adsorbed on $ACDCS_{optimal}$. The removal of Cr (VI) on $ACDCS_{optimal}$ was dependent on the pH of the solution. The pore filling, electrostatic attraction, reduction, and ion exchange were involved in the removal mechanism of Cr (VI) adsorbed on $ACDCS_{optimal}$. The metal leakage contents were traced. Accordingly, the prepared $ACDCS_{optimal}$ was a potential adsorbent for the removal of Cr (VI) from contaminated raw water.

Supplementary Materials: The following are available online at https://www.mdpi.com/article/10.3390/w13243602/s1, Figure S1: Van't Hof plot for the adsorption of Cr (VI) on $ACDCS_{optimal}$ (A); Fitting curve of activation energy for Cr (VI) adsorption on $ACDCS_{optimal}$ (B). Figure S2: SEM images of DCS (A), fresh CDCS (B), fresh $ACDCS_{optimal}$ (C) and $ACDCS_{optimal}$ with Cr (VI) adsorbed (D). Figure S3: (A) Survey XPS spectra of the fresh $ACDCS_{optimal}$ and $ACDCS_{optimal}$ with Cr (VI) adsorbed, (B) high resolution XPS spectra of the Cr2p peaks of $ACDCS_{optimal}$ with Cr (VI) adsorbed, and (C) high resolution XPS spectra of the C1s peaks of $ACDCS_{optimal}$ with Cr (VI) adsorbed, and (D) FTIR spectrum of fresh $ACDCS_{optimal}$ and $ACDCS_{optimal}$ with Cr (VI) adsorbed. Figure S4: Adsorption mechanism of Cr (VI) removal by $ACDCS_{optimal}$. Table S1: Results of the orthogonal test for ACDCS preparation and range analysis. Table S2: Elemental analysis and porosity characteristics of sample. Table S3: Contents of metal leakage from DCS and $ACDCS_{optimal}$.

Author Contributions: L.L.: Conceptualization, Methodology, Software, Formal analysis, Investigation, Data curation, Writing—original draft preparation. Y.L. (Yan Li): Resources. Y.L. (Yiqi Liu): Methodology. L.D.: Writing—review and editing, Project administration, Funding acquisition. X.J.: Supervision. H.L.: Supervision. J.Z.: Investigation. All authors have read and agreed to the published version of the manuscript.

Funding: This work was supported by the National Natural Science Foundation of China (Grant No. 51308001), Anhui Provincial Natural Science Foundation (Grant No. 2108085ME187), and the Open Project of Engineering Research Center of Biofilm Water Purification and Utilization Technology of Ministry of Education (Grant No. BWPU2020KF01).

Conflicts of Interest: The authors declare no conflict of interest.

References

1. Shen, C.; Zhao, Y.; Li, W.; Yang, Y.; Liu, R.; Morgen, D. Global profile of heavy metals and semimetals adsorption using drinking water treatment residual. *Chem. Eng. J.* **2019**, *372*, 1019–1027. [CrossRef]
2. Jia, M.; Peng, L.; Yang, M.; Wei, H.; Zhang, M.; Wang, Y. Carbon dots with dual emission: A versatile sensing platform for rapid assay of Cr (VI). *Carbon* **2021**, *182*, 42–50. [CrossRef]
3. Ding, L.; Jin, X.; Gao, Y.; Ma, J.; Zhang, X. Removal of Cr (VI) from Suddenly Polluted Raw Water Using Miex Resin: Parameters Optimization. *Fresenius Environ. Bull.* **2019**, *28*, 5052–5060.
4. Shahid, M.; Shamshad, S.; Rafiq, M.; Khalid, S.; Bibi, I.; Niazi, N.K.; Dumat, C.; Rashid, M.I. Chromium speciation, bioavailability, uptake, toxicity and detoxification in soil-plant system: A review. *Chemosphere* **2017**, *178*, 513–533. [CrossRef]
5. Sahinkaya, E.; Altun, M.; Bektas, S.; Komnitsas, K. Bioreduction of Cr(VI) from acidic wastewaters in a sulfidogenic ABR. *Miner. Eng.* **2012**, *32*, 38–44. [CrossRef]
6. Martín-Domínguez, A.; Rivera-Huerta, M.; Pérez-Castrejón, S.; Garrido-Hoyos, S.; Villegas-Mendoza, I.; Gelover-Santiago, S.; Drogui, P.; Buelna, G. Chromium removal from drinking water by redox-assisted coagulation: Chemical versus electrocoagulation. *Sep. Purif. Technol.* **2018**, *200*, 266–272. [CrossRef]
7. Dong, S.; Wang, Y.; Li, J.; Zhang, D.; Zhou, Y.; Tong, Y. Tuning the crosslink structure of cationic hydrogel for enhanced chromium(VI) removal: The covalent and electrostatic co-crosslinked effects and adsorption mechanism. *Chem. Eng. J.* **2020**, *394*, 124944. [CrossRef]
8. Basaran, G.; Kavak, D.; Dizge, N.; Aşçı, Y.; Şölener, M.; Ozbey, B.; Asci, Y. Comparative study of the removal of nickel(II) and chromium(VI) heavy metals from metal plating wastewater by two nanofiltration membranes. *Desalin. Water Treat.* **2015**, *57*, 21870–21880. [CrossRef]
9. Xiao, F.; Cheng, J.; Cao, W.; Yang, C.; Chen, J.; Luo, Z. Removal of heavy metals from aqueous solution using chitosan-combined magnetic biochars. *J. Colloid Interface Sci.* **2019**, *540*, 579–584. [CrossRef] [PubMed]
10. Min, X.; Li, Q.; Zhang, X.; Liu, L.; Xie, Y.; Guo, L.; Liao, Q.; Yang, Z.; Yang, W. Characteristics, kinetics, thermodynamics and long-term effects of zerovalent iron/pyrite in remediation of Cr(VI)-contaminated soil. *Environ. Pollut.* **2021**, *289*, 117830. [CrossRef]

11. Arroyo, M.; Pérez-Herranz, V.; Montañés, M.; Garcia-Anton, J.; Guiñón, J. Effect of pH and chloride concentration on the removal of hexavalent chromium in a batch electrocoagulation reactor. *J. Hazard. Mater.* **2009**, *169*, 1127–1133. [CrossRef] [PubMed]
12. Pantazopoulou, E.; Zebiliadou, O.; Noli, F.; Mitrakas, M.; Samaras, P.; Zouboulis, A. Utilization of Phosphogypsum in Tannery Sludge Stabilization and Evaluation of the Radiological Impact. *Bull. Environ. Contam. Toxicol.* **2014**, *94*, 352–357. [CrossRef]
13. Sun, Y.; Yue, Q.; Gao, B.; Gao, Y.; Li, Q.; Wang, Y. Adsorption of hexavalent chromium on Arundo donax Linn activated carbon amine-crosslinked copolymer. *Chem. Eng. J.* **2012**, *217*, 240–247. [CrossRef]
14. Wang, Y.; Wang, X.; Liu, M.; Wu, Z.; Yang, L.; Xia, S.; Zhao, J. Cr(VI) removal from water using cobalt-coated bamboo charcoal prepared with microwave heating. *Ind. Crops Prod.* **2012**, *39*, 81–88. [CrossRef]
15. Wu, J.; Yan, X.; Li, L.; Gu, J.; Zhang, T.; Tian, L.; Su, X.; Lin, Z. High-efficiency Adsorption of Cr(VI) and RhB by Hierarchical Porous Carbon Prepared from Coal Gangue. *Chemosphere* **2021**, *275*, 130008. [CrossRef] [PubMed]
16. Zhang, Y.; Tang, J.; Zhang, W.; Ai, J.; Liu, Y.; Wang, Q.; Wang, D. Preparation of ultrahigh-surface-area sludge biopolymers-based carbon using alkali treatment for organic matters recovery coupled to catalytic pyrolysis. *J. Environ. Sci.* **2021**, *106*, 83–96. [CrossRef]
17. Chen, T.; Zhou, Z.; Xu, S.; Wang, H.; Lu, W. Adsorption behavior comparison of trivalent and hexavalent chromium on biochar derived from municipal sludge. *Bioresour. Technol.* **2015**, *190*, 388–394. [CrossRef]
18. Li, M.; Zhou, J.; Bi, Y.-G.; Zhou, S.-Q.; Mo, C.-H. Polypyrrole/sewage sludge carbon as low-cost and high-effective catalyst for enhancing hexavalent chromium reduction and bio-power generation in dual chamber microbial fuel cells. *Sep. Purif. Technol.* **2020**, *256*, 117805. [CrossRef]
19. Mahapatra, U.; Chatterjee, A.; Das, C.; Manna, A.K. Adsorptive removal of hexavalent chromium and methylene blue from simulated solution by activated carbon synthesized from natural rubber industry biosludge. *Environ. Technol. Innov.* **2021**, *22*, 101427. [CrossRef]
20. Cheng, H.; Sun, Y.; Wang, X.; Zou, S.; Ye, G.; Huang, H.; Ye, D. Hierarchical porous carbon fabricated from cellulose-degrading fungus modified rice husks: Ultrahigh surface area and impressive improvement in toluene adsorption. *J. Hazard. Mater.* **2020**, *392*, 122298. [CrossRef]
21. Zhang, X.; Zhang, P.; Yuan, X.; Li, Y.; Han, L. Effect of pyrolysis temperature and correlation analysis on the yield and physicochemical properties of crop residue biochar. *Bioresour. Technol.* **2019**, *296*, 122318. [CrossRef]
22. Liang, Q.; Liu, Y.; Chen, M.; Ma, L.; Yang, B.; Li, L.; Liu, Q. Optimized preparation of activated carbon from coconut shell and municipal sludge. *Mater. Chem. Phys.* **2019**, *241*, 122327. [CrossRef]
23. Li, X.J.; Hao, J.Y. Orthogonal test design for optimization of synthesis of super early strength anchoring material. *Constr. Build. Mater.* **2018**, *181*, 42–48. [CrossRef]
24. Li, W.-H.; Yue, Q.-Y.; Gao, B.-Y.; Wang, X.-J.; Qi, Y.-F.; Zhao, Y.-Q.; Li, Y.-J. Preparation of sludge-based activated carbon made from paper mill sewage sludge by steam activation for dye wastewater treatment. *Desalination* **2011**, *278*, 179–185. [CrossRef]
25. Yang, B.; Liu, Y.; Liang, Q.; Chen, M.; Ma, L.; Li, L.; Liu, Q.; Tu, W.; Lan, D.; Chen, Y. Evaluation of activated carbon synthesized by one-stage and two-stage co-pyrolysis from sludge and coconut shell. *Ecotoxicol. Environ. Saf.* **2018**, *170*, 722–731. [CrossRef]
26. Wang, J.; Qiu, N.; Wu, H.; Wu, F.A. Preparation of Pruning Mulberry Shoot-based Activated Carbon by $ZnCl_2$ Activation. *Adv. Mater. Res.* **2011**, *282–283*, 407–411. [CrossRef]
27. Tu, B.; Wen, R.; Wang, K.; Cheng, Y.; Deng, Y.; Cao, W.; Zhang, K.; Tao, H. Efficient removal of aqueous hexavalent chromium by activated carbon derived from Bermuda grass. *J. Colloid Interface Sci.* **2019**, *560*, 649–658. [CrossRef]
28. Ma, H.; Yang, J.; Gao, X.; Liu, Z.; Liu, X.; Xu, Z. Removal of chromium (VI) from water by porous carbon derived from corn straw: Influencing factors, regeneration and mechanism. *J. Hazard. Mater.* **2019**, *369*, 550–560. [CrossRef]
29. Al-Othman, Z.; Ali, R.; Naushad, M. Hexavalent chromium removal from aqueous medium by activated carbon prepared from peanut shell: Adsorption kinetics, equilibrium and thermodynamic studies. *Chem. Eng. J.* **2012**, *184*, 238–247. [CrossRef]
30. Liu, H.; Liang, S.; Gao, J.; Ngo, H.H.; Guo, W.; Guo, Z.; Wang, J.; Li, Y. Enhancement of Cr(VI) removal by modifying activated carbon developed from Zizania caduciflora with tartaric acid during phosphoric acid activation. *Chem. Eng. J.* **2014**, *246*, 168–174. [CrossRef]
31. Duranoğlu, D.; Trochimczuk, A.W.; Beker, U. Kinetics and thermodynamics of hexavalent chromium adsorption onto activated carbon derived from acrylonitrile-divinylbenzene copolymer. *Chem. Eng. J.* **2012**, *187*, 193–202. [CrossRef]
32. Huang, D.; Wang, G.; Li, Z.; Kang, F.; Liu, F. Investigation of the removal mechanism of Cr(VI) in groundwater using activated carbon and cast iron combined system. *Environ. Sci. Pollut. Res.* **2017**, *24*, 18341–18354. [CrossRef]
33. Nasrullah, A.; Saad, B.; Bhat, A.; Khan, A.S.; Danish, M.; Isa, M.H.; Naeem, A. Mangosteen peel waste as a sustainable precursor for high surface area mesoporous activated carbon: Characterization and application for methylene blue removal. *J. Clean. Prod.* **2018**, *211*, 1190–1200. [CrossRef]
34. Nasrullah, A.; Bhat, A.; Naeem, A.; Isa, M.H.; Danish, M. High surface area mesoporous activated carbon-alginate beads for efficient removal of methylene blue. *Int. J. Biol. Macromol.* **2017**, *107*, 1792–1799. [CrossRef] [PubMed]
35. Zeng, Q.; Huang, Y.; Wang, H.; Huang, L.; Hu, L.; Zhong, H.; He, Z. A novel composite of almandine supported humboldtine nanospheres, in situ synthesized from natural almandine, possesses high removal efficiency of Cr(VI) over a wide pH range. *J. Hazard. Mater.* **2019**, *383*, 121199. [CrossRef] [PubMed]
36. Aghagoli, M.J.; Shemirani, F. Application of molybdenum disulfide nanosheets for adsorption of tetracycline in water samples. *Desalin. Water Treat.* **2017**, *70*, 250–260. [CrossRef]

37. Royer, S.; Duprez, D. Catalytic Oxidation of Carbon Monoxide over Transition Metal Oxides. *Chemcatchem* **2011**, *3*, 24–65. [CrossRef]
38. Weber, W.J.; Morris, J.C. Equilibria and Capacities for Adsorption on Carbon. *J. Sanit. Eng. Div.* **1964**, *90*, 79–108. [CrossRef]
39. Liu, W.; Zhang, J.; Zhang, C.; Ren, L. Preparation and evaluation of activated carbon-based iron-containing adsorbents for enhanced Cr(VI) removal: Mechanism study. *Chem. Eng. J.* **2012**, *189-190*, 295–302. [CrossRef]
40. Xu, Q.; Wang, Y.; Jin, L.; Wang, Y.; Qin, M. Adsorption of Cu (II), Pb (II) and Cr (VI) from aqueous solutions using black wattle tannin-immobilized nanocellulose. *J. Hazard. Mater.* **2017**, *339*, 91–99. [CrossRef]
41. Ding, L.; Wu, C.; Deng, H.; Zhang, X. Adsorptive characteristics of phosphate from aqueous solutions by MIEX resin. *J. Colloid Interface Sci.* **2012**, *376*, 224–232. [CrossRef] [PubMed]
42. Horsfall, M.J.; Spiff, A.I.; Abia, A. Studies on the Influence of Mercaptoacetic Acid (MAA) Modification of Cassava (Manihot sculenta Cranz) Waste Biomass on the Adsorption of Cu^{2+} and Cd^{2+} from Aqueous Solution. *Bull. Korean Chem. Soc.* **2004**, *25*, 969–976. [CrossRef]
43. Deng, C.; Liu, X.; Li, L.; Shi, J.; Guo, W.; Xue, J. Temporal dynamics of antibiotic resistant genes and their association with the bacterial community in a water-sediment mesocosm under selection by 14 antibiotics. *Environ. Int.* **2020**, *137*, 105554. [CrossRef] [PubMed]
44. Yue, Z.; Bender, S.E.; Wang, J.; Economy, J. Removal of chromium Cr(VI) by low-cost chemically activated carbon materials from water. *J. Hazard. Mater.* **2009**, *166*, 74–78. [CrossRef]
45. Gorzin, F.; Abadi, M.B.R. Adsorption of Cr(VI) from aqueous solution by adsorbent prepared from paper mill sludge: Kinetics and thermodynamics studies. *Adsorpt. Sci. Technol.* **2018**, *36*, 149–169. [CrossRef]
46. Zhang, W.; Zheng, J.; Zheng, P.; Qiu, R. Atrazine immobilization on sludge derived biochar and the interactive influence of coexisting Pb(II) or Cr(VI) ions. *Chemosphere* **2015**, *134*, 438–445. [CrossRef]
47. Hu, Y.; Yang, C.; Dan, J.; Pu, W.; Yang, J. Utilization of anaerobic granular sludge for chromium (VI) removal from wastewater: Optimization by response surface methodology. *Water Sci. Technol.* **2017**, *76*, 1112–1123. [CrossRef]
48. Liu, L.; Liu, X.; Wang, D.; Lin, H.; Huang, L. Removal and reduction of Cr(VI) in simulated wastewater using magnetic biochar prepared by co-pyrolysis of nano-zero-valent iron and sewage sludge. *J. Clean. Prod.* **2020**, *257*, 120562. [CrossRef]
49. Rai, M.; Shahi, G.; Meena, V.; Meena, R.; Chakraborty, S.; Singh, R.; Rai, B.N. Removal of hexavalent chromium Cr (VI) using activated carbon prepared from mango kernel activated with H_3PO_4. *Resour. Technol.* **2016**, *2*, S63–S70. [CrossRef]
50. Selvaraj, K.; Manonmani, S.; Pattabhi, S. Removal of hexavalent chromium using distillery sludge. *Bioresour. Technol.* **2003**, *89*, 207–211. [CrossRef]
51. Mohan, D.; Rajput, S.; Singh, V.K.; Steele, P.H.; Pittman, C.U. Modeling and evaluation of chromium remediation from water using low cost bio-char, a green adsorbent. *J. Hazard. Mater.* **2011**, *188*, 319–333. [CrossRef] [PubMed]